Evaluation of alternative fluence rate distribution models

Dong Liu, Joel Ducoste, Shanshan Jin and Karl Linden

ABSTRACT

A detailed evaluation of several fluence rate distribution models was performed. These models included line source integration (LSI), multiple points source summation (MPSS), multiple segment source summation (MSSS), UVCalc3D, RAD-LSI, view factor and discrete ordinate (DO). As part of the evaluation, a complete MSSS model, which accounts for the quartz sleeve thickness when calculating the refraction angles, was developed. In addition, a simple attenuation factor was introduced to integrate the physics of reflection, refraction and absorption effects into the LSI model. As an alternative simple correction to the LSI, the RAD-LSI incorporates the RADIAL intensity model into the original LSI formulation. All models were compared with experimental measurements using spherical actinometers, which measure the fluence rate at specific points in space. Experimental measurements were performed in air and water. Experiments in water were performed at two different ultraviolet transmittance (UVTs) (77 and 88%). The results showed that models that neglected the effects of refraction deviated significantly from the experimental data. In addition, the MSSS approach or models that incorporated the MSSS concept were found to best match the experimentally measured fluence rate distribution. Moreover, little difference was found between the results of MSSS with quartz sleeve thickness and UVCalc3D, which does not model the quartz sleeve thickness in the refraction angle calculation but uses a factor to account for the effects of the quartz sleeve on the fluence rate. The attenuation factor combined with the LSI model was found to match the MSSS model predictions, while reducing the computational cost.

Key words | disinfection, fluence rate, model, spherical actinometry, UV

Dong Liu
Joel Ducoste (corresponding author)
Department of Civil, Construction, and Environmental Engineering,
North Carolina State University,
208 Mann Hall CB 7908,
Raleigh, NC 27695-7908,
USA
E-mail: *jducoste@eos.ncsu.edu*

Shanshan Jin
Degremont North American Research & Development Center,
510 E. Jackson St,
Richmond, VA 23219,
USA

Karl Linden
Department of Civil and Environmental Engineering,
Duke University,
Durham, NC 27708-0287,
USA

INTRODUCTION

The use of ultraviolet light (UV) has been shown to be a cost-effective way to disinfect *Cryptosporidium* (Bolton *et al*. 1998; Bukhari *et al*. 1999), *Giardia* (Craik *et al*. 2001; Linden *et al*. 2002) and other pathogenic microorganisms in water treatment plants. One important criterion in UV disinfection is to assure that the UV system is delivering the appropriate UV fluence (dose). Although biodosimetry testing directly measures the UV reactor's performance, numerical simulations are useful in comparing reactor designs as well as estimating and improving the efficiency of disinfection processes; they provide a measure of the fluence distribution within a reactor and, more importantly, could be used to provide an estimate of the UV process performance where experimental validation cannot be conducted (Baas 1996; Lyn *et al*. 1999; Ducoste *et al*. 2003). As a result, it is important that the fluence rate distribution is known precisely throughout the UV reactor when mathematical modelling is used to predict the disinfection performance.

Characterizing the fluence rate from the lamp requires the incorporation of the principles of optics to the specific configuration of the reactor. Jacob and Dranoff (1970) developed the multiple points source summation (MPSS) approach, which is based on dividing the linear lamp into a series of n equally spaced point sources in an absorbing media. In the MPSS approach, the fluence rate from a specific point emanates uniformly in all directions (Figure 1a). Akehata and Shirai (1972) developed the

Downloaded from https://iwaponline.com/aqua/article-pdf/53/6/391/402516/391.pdf
by guest

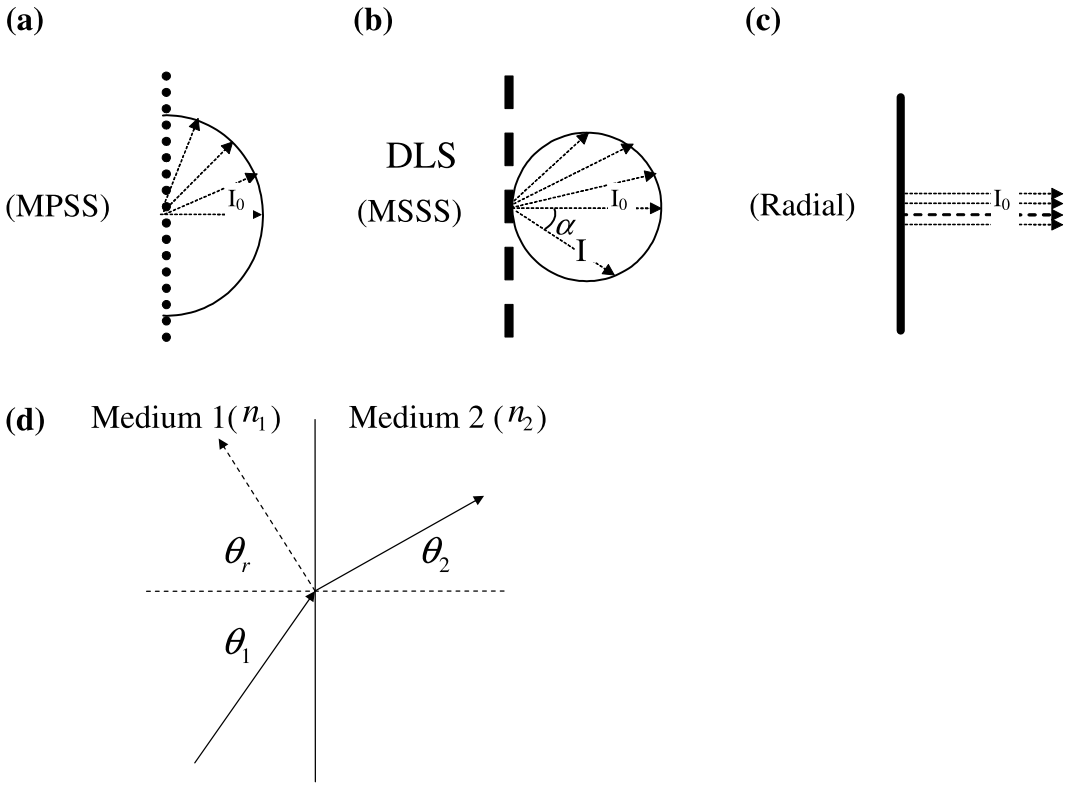

Figure 1 | Fluence rate production with (a) MPSS, (b) DLS or MSSS and (c) radial approaches, (d) refraction and reflection at the interface of two media with different refractive indices.

diffuse line source (DLS) model, which describes the fluence rate emanating from a series of points in the α-direction normal to the source axis as $I = I_0 \cos\alpha$, where I_0 is the normal fluence rate (Figure 1b). Akehata and Shirai compared the DLS model with the MPSS and radial (Figure 1c) models and found that the DLS model changed the shape and magnitude of the fluence rate distribution along the lamp length and in the radial direction.

Blatchley (1997) introduced the line source integration (LSI) model in which the MPSS model is integrated over an infinite number of point sources, producing a closed form solution when the absorbance of the medium is zero. The LSI and MPSS models are mathematically identical in the limit as the number of point sources, n, approaches ∞. However, in the case of an absorbing media, the LSI model is inappropriate and deviates from the MPSS model with decreasing UV transmittance. In addition, none of the previous models (Jacob and Dranoff, Akehata and Shirai, and Blatchley) incorporated reflection and refraction effects, which take place at the air/quartz/water interfaces.

Bolton (2000) improved the MPSS approach by developing a full version that accounted for reflection and refraction as well as absorption effects. Bolton showed that when the transmittance of water (T'_{10}) is much larger than 70%, the error associated with neglecting refraction and reflection can be as large as 25%. Bolton further showed that the number of point sources should be greater than 1,000 to produce an accurate representation of the lamp physics. As a result, the MPSS with refraction, reflection and absorption can be computationally intensive, especially when the UV system consists of several lamps or when a medium-pressure mercury lamp is used since it emits a broad range of wavelengths in the germicidal 200–300 nm band.

Bolton (2002, personal communication) further improved the MPSS model and introduced the multiple segment source summation (MSSS) method. The MSSS

Downloaded from https://iwaponline.com/aqua/article-pdf/53/6/391/402516/391.pdf
by guest

method incorporated much of the MPSS model including reflection, refraction and absorption described in a previous article (Bolton 2000). However, Bolton discovered that reflection, refraction and absorption did not completely correct for the over-prediction caused by modelling a lamp with a series of linear point sources as one approaches the lamp surface. The MSSS approach corrected for this over-prediction by modelling the lamp as a series of differential cylindrical segments, where light is emitted normal to the cylinder surface and decreases with the cosine of the angle between the unit normal vector and the direction vector. This cosine angle correction was similar to the DLS model of Akehata and Shirai (1972), but with the addition of reflection and refraction effects, and differed in the magnitude of I_0 shown in Figure 1b. Based on the MSSS method, Bolton developed a commercially available software for UV light intensity simulation, known as UVCalc3D. Bolton (2002, personal communication) reduced the computational requirement of the MSSS approach in UVCalc3D by developing a look-up table where the information for multiple lamps can be obtained from application of the MSSS approach for one lamp. However, UVCalc3D can still be computationally costly for multiple medium pressure lamps.

Another fluence rate distribution approach is the discrete ordinate (DO) method. DO is one of five methods for solving the radiative heat transfer equation that accounts for absorption and scattering effects when heat passes through a homogeneous and isotropic medium. Fiveland (1984) applied the DO approach to find numerical solutions in a two-dimensional rectangular enclosure with a grey absorbing, emitting and isotropically scattering medium. Stamnes *et al.* (1988) incorporated reflection, which takes place at the interface of the layers, into the DO method. Liou and Wu (1996) extended the DO method to the simulation of radiative transfer in a multi-layer medium with Fresnel interfaces, where the reflectivity is determined by Fresnel's equation. The model emphasized the importance of the angular dependence of reflectivity at the multi-layer interfaces and incorporated the effect of refraction. Hsu and coworkers also used the radiative transfer equation to model the propagation of light pulses in a three dimensional scattering media (Tan and Hsu 2001, 2002; Lu *et al.* 2003).

Also based on heat transfer, the view factor method was originally presented by Hamilton and Morgan (1952) in order to calculate the radiative heat transfer between two surfaces. Hsu (1967) derived a closed-form solution of the view factor for the general case of two arbitrary parallel rectangles. Modest (1993) demonstrated the use of view factor algebra for heat transfer between two co-axis cylinder surfaces and between surfaces of different shapes. Kowalski *et al.* (2000) calculated the UV irradiation intensity distribution in a chamber filled with air by using Modest's view factor algebra and considered the reflection effect of the chamber wall. However, the method was never demonstrated for use in an absorbing media.

While there do appear to be several methods for modelling fluence rate distribution, no prior study has performed a detailed side-by-side comparison with these different approaches. An objective of this research is to evaluate different fluence rate distribution methods. Blatchley (1997) demonstrated an experimental method of measuring the UV fluence rate through a collimator, which allows the radiometer detector surface to be struck by photons normal to it. Recent research by Rahn (1997), Linden and Mofidi (1999) and Rahn *et al.* (2000) has demonstrated the application of spherical actinometry for the measurement of germicidal radiation from monochromatic (low pressure) and polychromatic (medium pressure) UV sources. Because spherical actinometers act as 360° sensors, picking up photons from all angles, the number of photons incident on each sphere will be recorded inclusive of reflected and refracted radiation. As such, the spherical actinometry would better represent the fluence rate exposed by microorganisms. In this study, spherical actinometric experiments were performed and used to validate the fluence rate predictions at specific coordinates within the UV reactor.

In reactors where multiple medium pressure (MP) lamps are used, the computational requirements of utilizing an MPSS or MSSS modelling technique can be excessive. Another objective of this study was to investigate ways of reducing the computational cost of MPSS or MSSS based approaches, particularly when applied to multiple low pressure (LP) or MP UV systems. As a solution to this problem, a new approach utilizing an

Downloaded from https://iwaponline.com/aqua/article-pdf/53/6/391/402516/391.pdf
by guest

attenuation factor was developed. This approach was compared with the MSSS model.

Finally, since Bolton's UVCalc3D neglected the thickness of the quartz sleeve, which may cause some deviation for the refraction and reflection calculation at the air/quartz/water interfaces, a model, based on Bolton's MPSS and incorporating the quartz sleeve thickness, was investigated in this study. Other models that were also evaluated in this study include the MSSS, LSI, modified LSI, discrete ordinate method and view factor model. All models were applied in two testing lamp arrangements: one with air and one with water. Tests in water were performed at two UVT values: 77 and 88%.

OPTIC LAWS

Before analysing the refraction, reflection and absorption effects that occur at the air/quartz/water interfaces and the medium inside the reactor, it is important to understand some principles of optics used in the UV light intensity simulation.

Refraction (Snell's law)

Snell's law provides the relationship between incident angle, refractive angle and the refractive indices of two media. When the radiant energy passes through an interface between two media with different refractive indices (see Figure 1d), Snell's law is described as:

$$n_1 \sin\theta_1 = n_2 \sin\theta_2 \tag{1}$$

Reflection (Fresnel's law)

During the passage of radiant energy through an interface between two media of different refractive indices, a portion of the incident energy is reflected while the rest passes through the interface into the second medium (see Figure 1d). Based on the Fresnel's law (Meyer-Arendt 1984), the reflectance (R) for unpolarized incident energy is:

$$R = \frac{1}{2}[r_{II}^2 + r_{\perp}^2] \tag{2}$$

where, r_{II} is the amplitude of the radiant energy parallel to the plane of incidence and r_I is the amplitude of radiant energy perpendicular to the plane of incidence. Fresnel laws define these two amplitudes as

$$r_{II} = \frac{n_2 \cos\theta_1 - n_1 \cos\theta_2}{n_1 \cos\theta_2 + n_2 \cos\theta_1} \tag{3a}$$

$$r_{\perp} = \frac{n_1 \cos\theta_1 - n_2 \cos\theta_2}{n_1 \cos\theta_1 + n_2 \cos\theta_2} \tag{3b}$$

Inverse square law

At a distance r from a point source in a non-absorbing medium, the irradiance is given by the inverse square law as:

$$E = \frac{P}{4\pi r^2} \tag{4}$$

where, P is the radiant power uniformly emitted in all directions by the point source.

Absorption (Beer-Lambert law)

The irradiance in an absorbing medium can be calculated as:

$$E = E_0 U \tag{5}$$

where: E and E_0 are the irradiances with and without absorption, respectively, and U is the attenuation factor due to absorption. If $\alpha(\lambda)$ is the (napierian) absorption coefficient at wavelength λ, and l is the path length (cm), based on the Beer-Lambert law, the absorption attenuation factor U can be written as:

$$U = \exp[-\alpha(\lambda) l] \tag{6}$$

Downloaded from https://iwaponline.com/aqua/article-pdf/53/6/391/402516/391.pdf
by guest

In Equation (6), $\alpha(\lambda)$ is related to the absorbance. For a given wavelength λ, $A(\lambda)$ is described as:

$$A(\lambda) = \frac{\alpha(\lambda)l}{1\mathrm{n}(10)} \tag{7}$$

The transmittance, $T(\lambda)$, over the path length, l, is defined by

$$T(\lambda) = 10^{-A(\lambda)} \tag{8}$$

In practice, the transmittance is often measured using a 10 mm path length, and is designated by the symbol T'_{10}. From Equations 6 to 8, the relationship between attenuation factor U and the measured T'_{10} is computed as:

$$U = T'_{10}(\lambda)^{\frac{l}{l_{10}}} \tag{9}$$

where $l_{10} = 10$ mm.

FLUENCE RATE MODELS

MPSS model

This paper investigated the fluence rate distribution in a simplified UV disinfection system, which consists of a UV lamp inside a quartz sleeve mounted along the centre line of the reactor. Although the models presented in this research are for one-lamp simulations, since the fluence rates are spatially additive, multiple lamp UV systems can easily be incorporated.

The MPSS approach is based on the assumption that the emission of a linear lamp is equivalent to that of n point sources spaced equally along the axis of the lamp. As shown in Figure 2a, point A is one of the n point sources of the lamp, and point B is exposed to the UV light that comes from point A and passes through the air/quartz/water interfaces. The power output for each point source is P/n, where P is the total UV power output of the lamp in the wavelength band of interest. The overall value of the fluence rate at point B is then the sum of the values of the fluence rate calculated for each of the n point sources.

Figure 2a also illustrates the calculation of refraction angle for the fluence rate from point A to point B. h and r (Figure 2a) are the longitudinal and normal distances from B to A, respectively. r_1 is the normal distance from the axis line of the lamp to the inner surface of the quartz sleeve. r_2 is the thickness of the quartz sleeve and r_3 is the perpendicular distance from point B to the outer surface of the quartz sleeve. θ_1, θ_2, θ_3 are the refraction angles in the air, quartz and water, respectively, and d_1, d_2, d_3 are the path lengths of the UV light inside these media, respectively.

The three refraction angles are related by Snell's law as:

$$\sin(\theta_1)n_a = \sin(\theta_2)n_q = \sin(\theta_3)n_w \tag{10}$$

where, n_a, n_q, n_w are the refractive indices of the air, quartz and water, respectively.

In this study, common literature values were used for these indices such as $n_a = 1$, $n_q = 1.52$ and $n_w = 1.38$ (Bolton 2001). The refraction angles, r_i distances and h are related through the following equation:

$$\tan(\theta_1)r_1 + \tan(\theta_2)r_2 + \tan(\theta_3)r_3 = \mathrm{h} \tag{11}$$

Refraction angles θ_1, θ_2, θ_2 can be solved by combining Equations (10) and (11). The path lengths d_1, d_2, d_3, of UV light in the different media are related to the refraction angles by:

$$d_1 = r_1/\cos(\theta_1) \tag{12a}$$

$$d_2 = r_2/\cos(\theta_2) \tag{12b}$$

$$d_3 = r_3/\cos(\theta_3) \tag{12c}$$

After considering reflection at the air/quartz/water interfaces and absorption through the different media, the calculation of the fluence rate from point source A to point B can be written as:

$$I_A = (1-R_1)(1-R_2)\frac{P/n}{4\pi(d_1+d_2+d_3)^2}T_w^{d_3/0.01}T_q^{d_2/0.01}\ (W/m^2) \tag{13}$$

Downloaded from https://iwaponline.com/aqua/article-pdf/53/6/391/402516/391.pdf
by guest

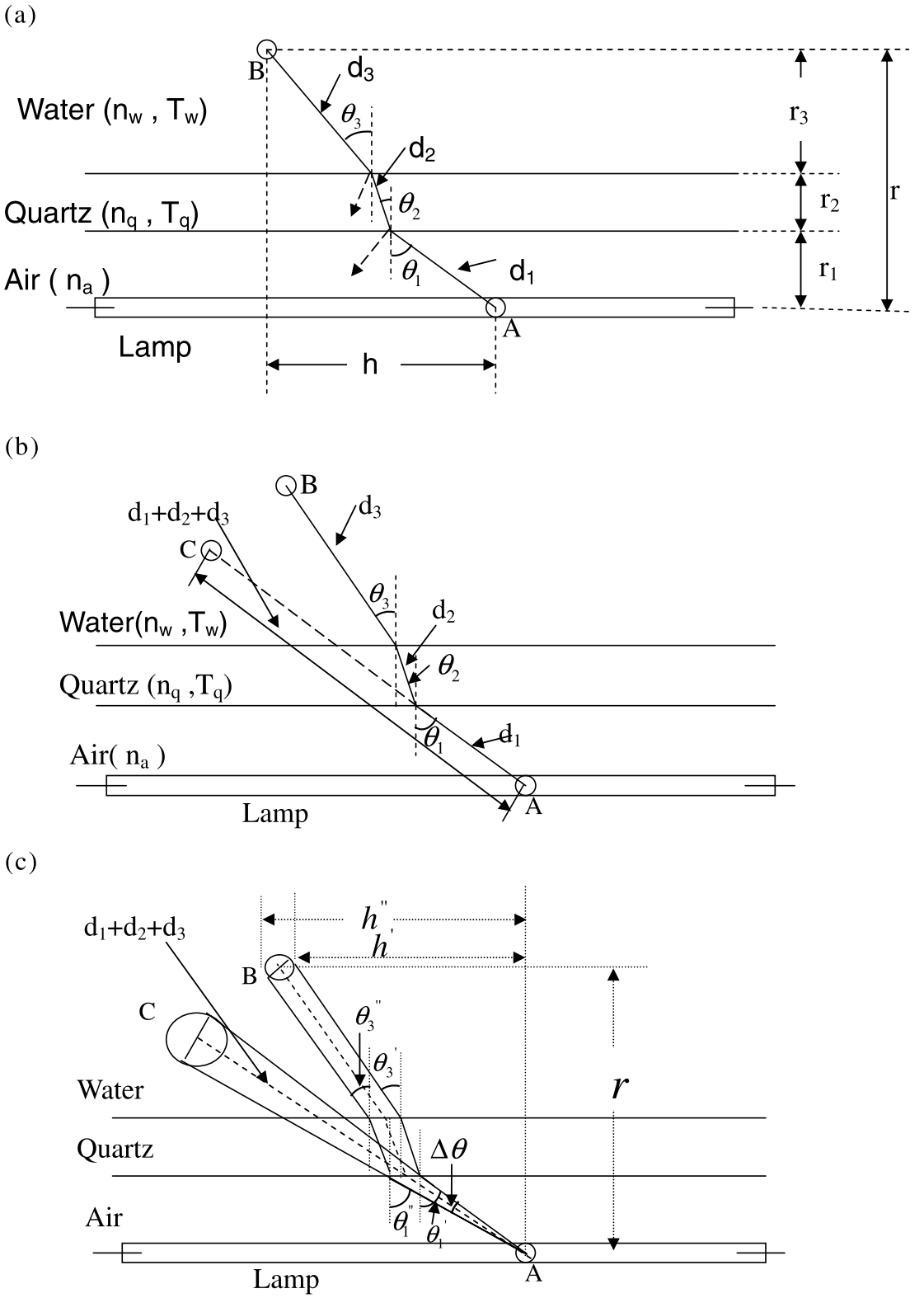

Figure 2 | Components of refraction: (a) refraction angle calculation, (b) bending effect and (c) focus effect.

Downloaded from https://iwaponline.com/aqua/article-pdf/53/6/391/402516/391.pdf
by guest

In Equation 13, R_1 and R_2 are the reflectance factors for the air/quartz and quartz/water interfaces, respectively, and can be derived from the Fresnel's law (Equations 2 and 3). T_w and T_q are the 10 mm path length transmittance of the water and quartz, respectively. In Equation (13), the unit of the path length d_1, d_2 and d_3 must be meters. Equation (13) incorporates the bending effect for refraction, which is shown in Figure 2b. The refraction effect, taking place at the air/quartz/water interfaces, shifts point C to point B. Therefore, a bending effect changes the fluence rate spatial distribution significantly when compared with conditions without refraction.

In addition to the bending effect, another component of the refraction is the focus effect, which is illustrated in Figure 2c. The output power emitted from point A within the finite difference angle, $\Delta\theta$, would normally reach point C with a different cross-sectional area exposed to the UV light compared with point B, when refraction is not considered. In other words, the focus effect of refraction concentrates the light power from a larger cross-sectional area at point C to a smaller one at point B. In this paper, we introduce a new parameter called the focus factor (*Focus*), which is used to represent the concentrating effect caused by refraction.

In Figure 2c, the dashed lines represent the path of UV light coming from point A to point B and to point C with and without the refraction, respectively. The finite difference angle, $\Delta\theta$, is related to the refraction angles θ_1, θ_2, and θ_3 by:

$$\theta_1 = \theta_1'' - \frac{\Delta\theta}{2} = \theta_1' + \frac{\Delta\theta}{2} \tag{14}$$

Based on cylindrical symmetry to the axis of the lamp, the focus factor can be obtained by dividing the cross-sectional area of a circular segment between the finite difference angle ($\Delta\theta$) without refraction, by that with refraction. For the case without refraction, the cross-sectional area of the circular segment, which is exposed to the light in the finite difference angle $\Delta\theta$, is:

$$A_{wo} = 2\pi(d_1 + d_2 + d_3)^2 \Delta\theta \cos\theta_1 \tag{15}$$

The cross-sectional area with refraction can be expressed as:

$$A_w = 2\pi r(h'' - h')\cos\theta_3 \tag{16}$$

where, h'' and h' are given by Equations (10) and (11).

The focus factor is then calculated as:

$$Focus = \frac{A_{wo}}{A_w} = \frac{(d_1+d_2+d_3)^2 \Delta\theta \cos\theta_3}{r(h''-h')\cos\theta_3} \tag{17}$$

The fluence rate at point B that arises from point source A taking into account reflection and absorption, as well as bending and focus effects of refraction is:

$$I_A = (1-R_1)(1-R_2) \frac{P/n}{4\pi(d_1+d_2+d_3)^2} T_w^{d_3/0.01} T_q^{d_2/0.01} Focus\ (W/m^2) \tag{18}$$

MSSS model

The MSSS model incorporates much of the MPSS model including reflection, refraction and absorption as described in Equation (18). However, Bolton (2002, personal communication) discovered that reflection, refraction and absorption did not completely correct for the over-prediction caused by modelling a lamp with a series of point sources at regions near the lamp surface and near the lamp ends. Bolton corrected for this over-prediction by simulating the lamp as a series of differential cylindrical segments, where light is emitted normal to the cylinder surface and decreases with the cosine of the refraction angle θ_1. Based on the MSSS model for the configuration shown in Figure 2, the fluence rate at point B caused by the UV light emitted from segment source A can be written as:

$$I_A = (1-R_1)(1-R_2) \frac{P/n}{4\pi(d_1+d_2+d_3)^2} T_w^{d_3/0.01} T_q^{d_2/0.01} Focus \cos\theta_1\ (W/m^2) \tag{19}$$

Bolton (2002, personal communication) has incorporated the MSSS approach into commercially available software, known as UVCalc3D. The main difference between UVCalc3D and Equation (19) is the inclusion of the quartz sleeve in calculating the refraction effects. UVCalc3D omitted the thickness of the quartz sleeve

Downloaded from https://iwaponline.com/aqua/article-pdf/53/6/391/402516/391.pdf
by guest

while calculating the refraction angles, and uses a simple factor to describe the effect of quartz sleeve on the fluence rate distribution. In this study, both Equation (19) and UVCalc3D were used to model the fluence rate distribution inside a test reactor filled with water to investigate the significance of the quartz sleeve in the refraction angle calculations.

LSI model

The LSI model is the continuous (integral) version of the MPSS model (Blatchley 1997). The LSI and MPSS models are mathematically identical in the limit as the number of point sources, n, approaches ∞. LSI is an efficient approach to the MPSS method in that a closed-form solution exists and that there is no need for a numerical routine. However, the closed form solution only exists in the absence of absorption, reflection and refraction. The LSI fluence rate at a point with a normal distance R from the lamp and a longitudinal distance H from the centre of the lamp with length L is given as:

$$I = \frac{P}{4\pi LR}\left[arctan\left(\frac{L/2+H}{R}\right)+arctan\left(\frac{L/2-H}{R}\right)\right] \tag{20}$$

In this study, Equation (20) was used to model the fluence rate distribution emitted from a lamp in air, where absorption, reflection and refraction can be omitted.

Attenuation factor approach

Although Equation (20) does not include absorption, reflection and refraction effects, it is much simpler than the MPSS model and significantly less computationally intensive. Unfortunately, it was not designed to include the important physics of reflection, absorption and refraction (i.e. bending and focus) of light. In this study, a simplified version of the MPSS was developed by multiplying Equation (20) by an attenuation factor. The attenuation factor is calculated by dividing an n-points MPSS model (or MSSS model) that accounts for reflection, refraction and absorption by an n-points MPSS model without any of these effects. The use of the attenuation factor is shown in Equation (21) along with Equation (22):

$$I = \frac{P}{4\pi LR}\left[arctan\left(\frac{L/2+H}{R}\right)+arctan\left(\frac{L/2-H}{R}\right)\right] \times (atten\ factor) \tag{21}$$

where:

$$(atten\ factor)_{b,f} = \sum_{k=1}^{n}(1-R_{1,k})(1-R_{2,k}) \frac{\frac{P/n}{4\pi(d_{1,k}+d_{2,k}+d_{3,k})^2}T_w^{d_{3,k}/0.01}T_q^{d_{2,k}/0.01}Focus_k}{\sum_{k=1}^{n}\frac{P/n}{4\pi(r_k^2+h_k^2)}} \tag{22a}$$

$$(atten\ factor)_{b} = \sum_{k=1}^{n}(1-R_{1,k})(1-R_{2,k}) \frac{\frac{P/n}{4\pi(d_{1,k}+d_{2,k}+d_{3,k})^2}T_w^{d_{3,k}/0.01}T_q^{d_{2,k}/0.01}}{\sum_{k=1}^{n}\frac{P/n}{4\pi(r_k^2+h_k^2)}} \tag{22b}$$

$$(atten\ factor)_{b,f,c} = \sum_{k=1}^{n}(1-R_{1,k})(1-R_{2,k}) \frac{\frac{P/n}{4\pi(d_{1,k}+d_{2,k}+d_{3,k})^2}T_w^{d_{3,k}/0.01}T_q^{d_{2,k}/0.01}Focus_k\cos\theta_{1,k}}{\sum_{k=1}^{n}\frac{P/n}{4\pi(r_k^2+h_k^2)}} \tag{22c}$$

The variables used in the attenuation factor are shown in Figure 3. The ratio in Equation (22) describes the amount of light reduction due to reflection, refraction and absorption. In Equation (22a), both the bending and focus effects of refraction are included. However, the numerator of the attenuation factor can be derived from Equation (13), which corresponds to the MPSS model without the focus effect of refraction, and from Equation (19), which represents the MSSS model. Equations (22b) and (22c) represent the attenuation factors that were based on these two methods.

Downloaded from https://iwaponline.com/aqua/article-pdf/53/6/391/402516/391.pdf
by guest

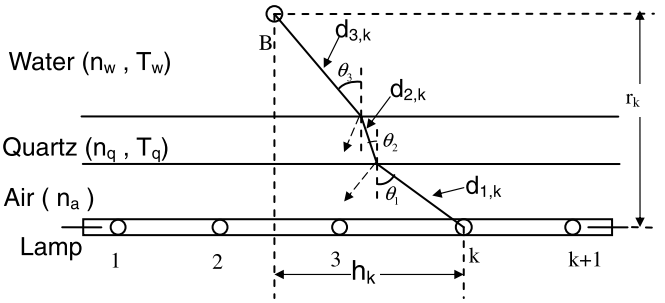

Figure 3 | Illustration of the attenuation factor calculation.

Equation (22b) can be combined with fluence rate distribution models (i.e. RAD-LSI and view factor) where the focus effect will incorrectly describe the longitudinal profiles near the quartz sleeve surface with these models. In this study, three values of n = 3, 5 and 10, were used to determine the resolution for the attenuation factor in Equation (22). The fluence rate computed using Equations (21) and (22c) was compared with the MSSS model, which used 1,000 segment sources.

Modified LSI (RAD-LSI)

The closed-form of the LSI model has been shown to be effective for simulating far-field fluence rate distribution (Blatchley 1997). However, the disagreement between the experimental measurements and model predictions will increase as the probe approaches the quartz sleeve surface. Since Bolton (2002, personal communication) realized that a portion of the fluence rate was emitted in the radial direction for linear lamps, a model for the radial intensity calculation was incorporated into the LSI as a simple modification to account for the radial direction of the fluence rate as one approaches the lamp surface. Equation (23) displays the modified LSI, known as RAD-LSI.

$$I = \underset{\text{I}}{minimum}\left\{\underset{\text{A}}{\frac{P}{2\pi LR}}, \underset{\text{B}}{\frac{P}{4\pi LR}\left[arctan\left(\frac{L/2+H}{R}\right)+arctan\left(\frac{L/2-H}{R}\right)\right]}\right\}*(atten\ factor)_b \quad (23)$$

The first part of the minimum function in Equation (23) (I A) represents the fluence rate based on the radial intensity model. Part (I B) is the original LSI model. In order to include the absorption, reflection and refraction effects, Equation (23) was multiplied by the attenuation factor based on Equation (22b).

DO (discrete ordinate) method

The DO method is one of five numerical approaches for solving the radiative transfer equation (Equation 24), which accounts for radiation in an absorbing medium.

$$\underset{\text{I}}{(\Omega\bullet\nabla)I(r,\Omega)} = \underset{\text{II}}{-(k_a+k_s)I(r,\Omega)}\underset{\text{III}}{}+\underset{\text{IV}}{k_aI_b(r)} + \frac{k_s}{4\pi}\int_{\Omega'=4\pi}\underset{\text{V}}{I(r,\Omega')\theta(\Omega'\rightarrow\Omega)d\Omega'} \quad (24)$$

where Ω is direction of propagation of radiation beam; k_a, k_s absorption and scattering coefficients (1 m^{-1}); I_b is intensity of black body radiation; and φ is scattering phase function.

As shown in Equation (24), part I of the radiative transfer equation is the gradient of intensity along the propagation direction, part II is the loss due to absorption, part III is the loss due to out-scattering, part IV is the gain due to black-body emission, and part V is the gain due to in-scattering. Although Equation (24) was originally proposed for the heat transfer in one medium, several researchers (Stamnes *et al*. 1988; Liou and Wu 1996) have improved it to model radiative transfer in the multi-layer medium with fresnel interfaces. In this study, a commercially available software, known as FLUENT (Lebanon, New Hampshire), which has a built-in version of the DO model to solve the radiative transfer equation, was used to predict the fluence rate distribution inside a reactor filled with water. FLUENT's version of the DO model does not include the refraction effect of light. In the current model set-up, the scattering terms were neglected since no particles were present in the experimental system.

View factor method

The view factor approach was primarily used to determine the radiant heat transfer between two arbitrarily sized

Downloaded from https://iwaponline.com/aqua/article-pdf/53/6/391/402516/391.pdf
by guest

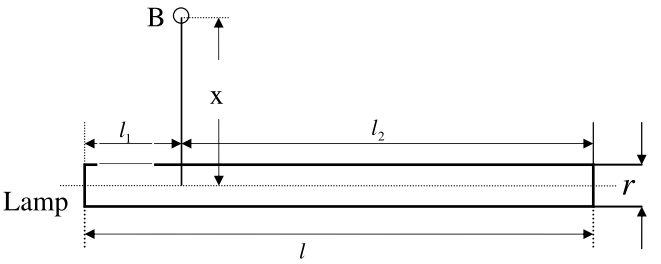

Figure 4 | Illustration for view factor method.

parallel rectangles. Based on the idea of the view factor algebra, Modest (1993) developed a model to calculate the irradiance intensity from a cylindrical surface to a differential element in space. Kowalski *et al.* (2000) applied the view factor approach to simulate the light intensity field for the prediction of disinfection in air streams. The basic theory underlying the view factor approach is that a cylindrical lamp can be divided into two parts according to the location of the point of interest. For each lamp section, the view factor method predicts the fraction of radiation emitted from the surface of the lamp section that directly strikes a differential element. The intensity at any point is the product of the view factor and the surface intensity of the lamp. The surface intensity is simply the UV power output in watts divided by the lamp surface area. As illustrated in Figure 4, the view factor approach is calculated as:

$$F_i = \frac{L_i}{\pi H}\left[\frac{1}{L_i}ATAN\left(\frac{L_i}{\sqrt{H^2-1}}\right)+ \frac{X_i-2H}{\sqrt{X_iY_i}}ATAN\left(\sqrt{\frac{X_i(H-1)}{Y_i(H+1)}}\right)-ATAN\left(\sqrt{\frac{H-1}{H+1}}\right)\right] \quad (25)$$

where, $H = x/r$; $L_i = l_i/r$; $X_i = (1+H)^2 + L_i^2$; $Y_i = (1-H)^2 + L_i^2$; and $i = 1,2$.

The light intensity is then determined by:

$$I = I'(F_1 + F_2) \quad (26)$$

In Equation (26), I' is the surface intensity of the lamp, and is calculated as:

$$I' = \frac{P}{2\pi rl} \quad (27)$$

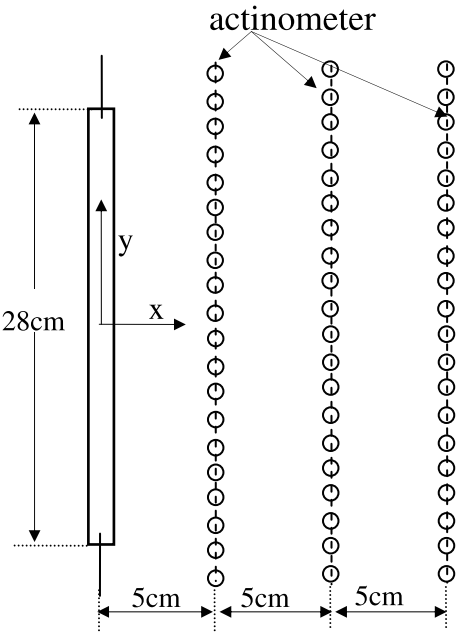

Figure 5 | Schematic illustration of test reactor in the air.

Equations (25–27) alone do not account for absorption, reflection and refraction effects. These effects were included in the view factor approach by multiplying Equation (26) by Equation (22b) to simulate the fluence rate distribution inside a reactor filled with water. With the exception of the DO method and UVCalc3D, all other fluence rate models were incorporated in commercially available computational fluid dynamics software, PHOENICS (CHAM, CAMBRIDGE, UK).

EXPERIMENTAL METHOD

Test reactors

In this study, actinometry measurements and numerical simulations of the fluence rate inside two test reactors were performed to validate these different mathematical models. Figure 5 displays the reactor configuration for tests conducted in air. Solutions of the potassium iodide/iodate (KI) actinometer (Rahn 1997) were housed in spherical quartz containers and suspended parallel to a low pressure (LP) mercury UV lamp at three specific positions with radial distances of 5, 10 and 15 cm from the

Downloaded from https://iwaponline.com/aqua/article-pdf/53/6/391/402516/391.pdf
by guest

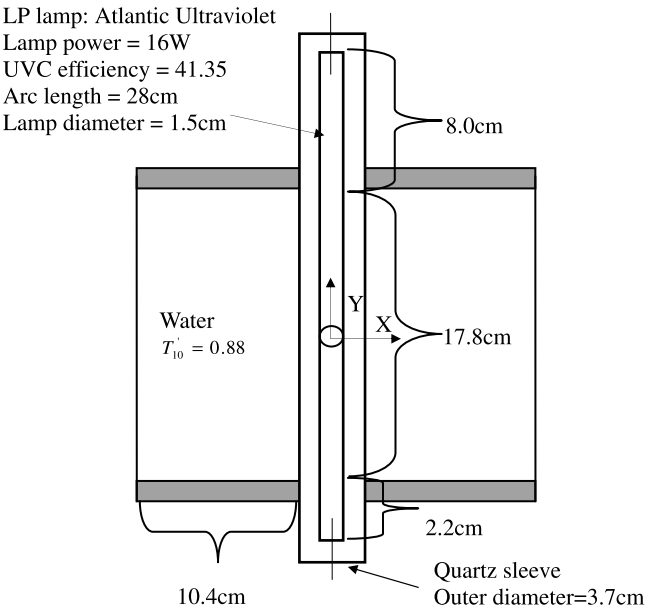

Figure 6 | Nickel plated stainless steel reactor filled with water for transmissivity tests.

lamp. The arc length of the LP lamp used in this study was 28 cm and the total output power at the 254 nm wavelength band was 16 watts with a measured UVC efficiency of 41.35%.

The 16 W of lamp electrical power was obtained from the lamp manufacturer. The UVC output power was measured using an International light IL1700 radiometer at a distance of 1.5 m from the lamp centreline in air. The radiometer was calibrated for 253.7 nm. A distance of 1.5 m is greater than four times the electrode-to-electrode length of the lamp (28 cm). The radiometer sensor was assumed to receive radiation from a point source. The fluence rate was therefore assumed to fall off as the inverse square of the distance between the sensor plate of the radiometer and the centre point of the lamp. UVC output power was then calculated by: radiometer reading (mW cm^{-2}) × 4 (pi) 150^2 cm^2.

Transmissivity tests were performed inside a reactor filled with water as shown in Figure 6. A KI actinometer in spherical quartz vessels was suspended at 18 locations in water with 77 and 88% UV transmittance (UVT) at 254 nm. These two UVT values were used in this study because they cover a range of UV transmittance that would be typical of a good quality wastewater and moderate quality water UV disinfection application. The centre point of the reactor was chosen as the origin of the coordinate system. The X and Y axes are the directions perpendicular and parallel to the lamp, respectively.

A 0.1 M KIO_3/0.6 M KI in 0.01 M $Na_2B_4O_7 \cdot 10H_2O$ (Fisher scientific) solution was freshly made as the KI/KIO_3 actinometer. Fluence rates (mW cm^{-2}) were calculated using the following equation (Rahn 1997):

$$Fluence\ rate = \frac{\Delta a_{352} V}{\Phi_\lambda \varepsilon A_{cs} t(1-R)} \times U \quad (28)$$

where:

Φ_λ = quantum yield for generation of I_3^- at average light emission ($0.64 \times [1 + 0.02 \times (T - 20.7)]$ moles/Einstein)

T = actinometer temperature during irradiation (°C)

Δa_{352} = change of absorption coefficient at 352 nm (cm^{-1})

ε = molar absorption coefficient at 352 nm (26,400 M^{-1} cm^{-1})

V = volume of irradiated actinometer solution (l)

A_{cs} = cross-sectional area of the spherical vessels (cm^2)

U = constant used to convert Einstein into conventional UV fluence units (4.7153×10^8 mJ $einstein^{-1}$ for LP based on 253.7 nm emission)

t = UV exposure time (s)

R = reflection of quartz vessel surface

Note that in the calculated fluence value, the molar absorption coefficient of 26,400 M^{-1} cm^{-1} was obtained from Rahn (1997). However, a recent study determined the molar absorption coefficient of I_3^- in the actinometer solution to be 27,636 M^{-1} cm^{-1} (Stefan *et al.* 2001). The differences in the data presented when evaluated using these two approaches results in a 5% overestimation using the Rahn (1997) values. In the calculation, the reflection of light by the quartz is also taken into consideration. The reflection was calculated based on the approach developed by Bolton (2000). For this study, the reflection of light by the quartz vessel was calculated as 8.9% and 0.4% in air and water, respectively (Bolton 2003, personal communication).

Downloaded from https://iwaponline.com/aqua/article-pdf/53/6/391/402516/391.pdf
by guest

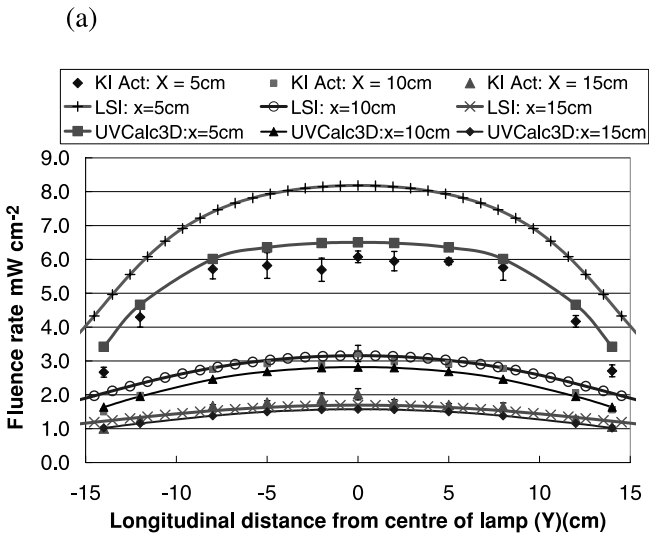

Figure 7 | Fluence rate distribution along the lamp at different normal distance to the lamp (x=5, 10, 15 cm): (a) impact of LSI, (b) impact of RAD-LSI.

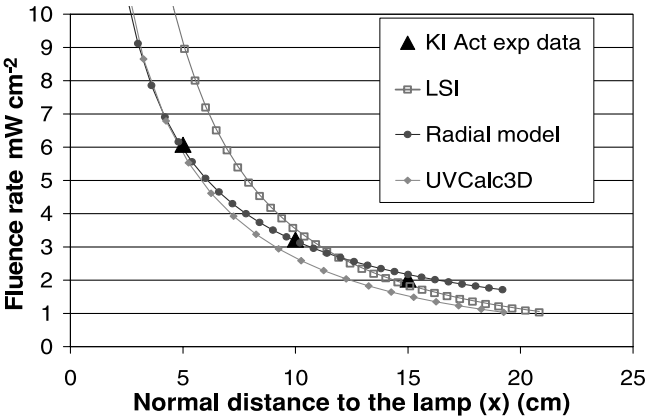

Figure 8 | Fluence rate radial distribution on the profile of the centre point of the lamp.

RESULTS AND DISCUSSION

Fluence rate distribution in air

Figures 7 and 8 display the fluence rate distribution in the air box. The error bar on the KI/KIO_3 actinometer test data curve represents the experimental standard deviation. In Figure 7a, the results show that the LSI model predicted a higher fluence rate than both the experimental measurements and the UVCalc3D model at a radial distance of 5 cm. Far from the lamp (x = 10 and 15 cm), both of these mathematical models agreed well with the experimental data. Modifications made to the original LSI model, RAD-LSI, were found to improve the fluence rate distribution predictions at x = 5 cm (Figure 7b), while maintaining the same level of accuracy far from the lamp. As discussed earlier, the LSI model displays a higher fluence rate distribution in the region close to the lamp centre. This higher fluence rate is due to the point source assumption, which does not consider the cylindrical geometry of the UV lamp. In a cylindrical geometry configuration, light is emitted predominantly in the radial direction while the point source approximation assumes a uniform light emission in all directions. The RADIAL portion of the RAD-LSI seems to provide a simple correction for the fluence rate around the lamp central region.

Figure 8 clearly shows the improvement of the RAD-LSI model as one approaches the lamp surface. RAD-LSI selects either the RADIAL model or the LSI model to determine the fluence rate based on the location of the point of interest. Near the lamp surface, the RADIAL model predicts a lower fluence rate than the LSI model. However, near the lamp ends and at radial distances further from the lamp surface, the LSI model predicts a lower fluence rate than the RADIAL model. Unfortunately, the RAD-LSI still has problems predicting the fluence rate near the lamp ends because of the point source approximation of the LSI portion. UVCalc3D's ability to better predict experimental fluence rate results

Downloaded from https://iwaponline.com/aqua/article-pdf/53/6/391/402516/391.pdf
by guest

suggests that the cosine angle effect is important in characterizing the fluence rate near the lamp.

Although not reported in the figures, the view factor approach was found to produce similar results to RAD-LSI with the exception of near the lamp ends. In that region, the view factor model was closer to the experimental results but still above the UVCalc3D predictions. The view factor model's improvement over the LSI model is due to its inclusion of cylinders as its source of light emission and not a series of point sources (Modest 1993). However, like the RAD-LSI, the view factor model fails to predict regions near the lamp ends because it does not account for the non-uniform emission pattern in the derivation of Equation (25), which accounts for the fraction of irradiation on the differential element (Modest 1993). Overall, the fluence rate results in air suggest that the lamp is best approximated by using the MSSS concept.

Fluence rate distributions in water

Figure 9 displays the fluence rate distribution prediction at the 18 measurement points in a reactor filled with water. The modelling results were compared with experimental measurements at 77 and 88 UVTs. However, only the 88 UVT results were displayed in Figure 9 since the trends seen at 88 UVT were also found at 77 UVT. The goodness of fit between the experimental and modelling results was computed as (Kvalseth 1985):

$$R^2 = 1 - \sum_{i=1}^{18} (I_i - \hat{I})^2 / \sum_{i=1}^{18} (I_i - \bar{I}) \tag{29}$$

where I_i represents the experimental results, $\bar{I}$ is the average value of I_i over all of the points and $\hat{I}_i$ represents the model results. In Figure 9a, for test points (1, 2, 4, 5 and 6) far from the lamp, the MSSS model, UVCalc3D and RAD-LSI were found to under-predict the experimental fluence rate and yield similar results. Essentially, the transmissivity tests were conducted in a metallic reactor where the interior wall surface was smooth with a high surface finish. As a result of this metallic wall condition, some of the fluence rate emanating from the lamp was reflected back into the fluid from the wall. Currently, the models presented in this study do not include terms that account for wall reflection; however, the quartz vessels with actinometer solution would measure this reflected radiation.

Quartz vessels at positions 1, 2, 4, 5 and 6 were placed fairly close to the reactor wall (i.e. centre of the quartz vessel was 0.7 cm from the wall) while the quartz vessel at position 3 was placed 3 cm from the wall. As the results in Figure 9a show, it is reasonable to conclude that a portion of the fluence rate contribution to points 1, 2, 4, 5 and 6 is from wall reflection due to these points' close proximity to the wall. The portion of the measured fluence rate resulting from wall reflection decreases as the measurement location moves away from the wall as with position 3. The results at points 1, 2, 4, 5 and 6 suggest that wall reflection could play an important role in the accurate prediction of the low dose region of a dose distribution curve in a UV reactor. Without wall reflection, the MSSS model, UVCalc3D and RAD-LSI were found to predict the low dose region reasonably well within 20% of the mean and inside the error bar limits as shown with position 3.

At the intermediate measurement points (test points 7–12, Figure 9a) all three models exhibited reasonable agreement with the experimental data. In the region close to the lamp (points 13–18) the fluence rate predictions from both the MSSS model and UVCalc3D were more accurate than RAD-LSI. The difference between calculated and measured results was quite large at test point 14 (Figure 9a). However, considering the fluence rate value at point 13, which is located further from the lamp centre and yields even higher UV light intensity than point 14 in the actinometer measurement, it is likely that the disagreement between numerical and experimental results may have been caused by saturation of the actinometer solution at point 14. Because the solution in the spherical vessel is not mixed during the irradiation, it is possible that the high UV fluence rate produced a 'saturation' effect of the actinometric solution in the inner quartz surface of the spherical vessels (Sommer *et al.* 1999). Under saturated conditions, the spherical actinometer underestimates the fluence rate. The MSSS model differs with UVCalc3D only with the inclusion of the quartz sleeve thickness when calculating the refraction angle. The results in Figure 9a

Downloaded from https://iwaponline.com/aqua/article-pdf/53/6/391/402516/391.pdf
by guest

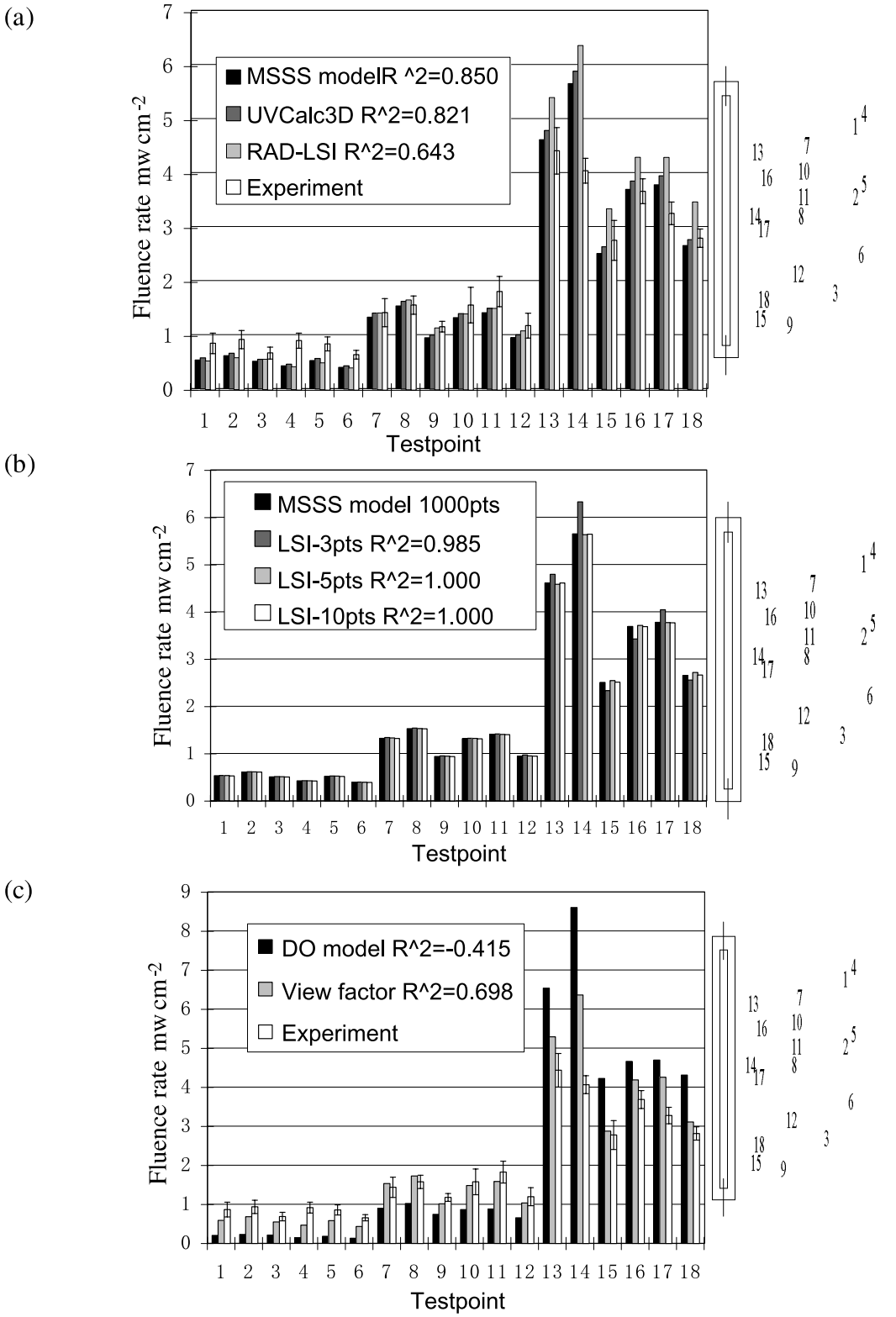

Figure 9 | Fluence rate value in water at test points: (a) comparison between UV Calc3D, RAD-LSI and MSSS models, (b) determination of appropriate n value for attenuation factor, (c) comparison between DO and view factor models.

Downloaded from https://iwaponline.com/aqua/article-pdf/53/6/391/402516/391.pdf
by guest

seem to suggest that the inclusion of the quartz sleeve thickness is insignificant and therefore can be approximated by a factor in any future modelling approach as computed in UVCalc3D.

Figure 9b compares the MSSS model with the LSI model that incorporates the attenuation factor (Equation 22c) using 3, 5 and 10 points approximation. The goal here was to determine the number of points needed in the attenuation factor calculation. Each n point approach was compared with the MSSS approach also using Equation (29). For this calculation, I_i represents MSSS model results and $\hat{I}_i$ represents the LSI model results using different n values for the attenuation factor. In Figure 9b, all three n values yield very high R^2 values suggesting that all three n values could be used to approximate the MSSS approach. Looking at regional differences, the results show that the 3, 5 and 10 points attenuation factors yield identical results at locations far from the lamp. Near the lamp, the greatest deviation occurred between the three-point approximation and the MSSS model. The results suggest that the five-point approximation method for attenuation factor calculation is a time efficient and accurate alternative to the MSSS model. As a result, the five-point approximation was applied to other attenuation factor calculations used in this study.

Figure 9c displays a comparison of the DO and view factor models with the experimental results. In Figure 9c, the large difference between the DO model and the experimental data can be attributed to neglecting both bending and focus effects of refraction at air/quartz/water interfaces. As mentioned earlier, the commercial software, FLUENT, only accounts for absorption and scattering when solving the radiative transport equation (Equation 25). Scattering was neglected since no particles were present in the experimental tests. The inaccuracy of the DO model demonstrates the significance of the refraction effect when dealing with water. Bolton (2000) discusses the influence of refraction when calculating the fluence rate distribution in UV systems for drinking water disinfection. Bolton shows that when the UVT is much larger than 70%, neglecting refraction will cause large errors for point source summation methods. Although the DO model is based on a different method from that of the point source summation method, ignoring refraction still resulted in large errors.

As a result, refraction effects should be incorporated into the DO model in FLUENT to improve its performance. In Figure 9c, the view factor model combined with the five-points attenuation factor based on Equation (22b) predicted comparable results to the RAD-LSI, MSSS and UVCalc3D. Like the DO model, the view factor model is not derived from the point source summation method. However, owing to the introduction of the attenuation factor, which covers reflection, refraction and absorption effects, its result was relatively closer to the actinometer measurement data than the DO model.

Figure 10a–d displays the longitudinal shape of different fluence rate distribution models along the lamp length at different radial distances ($x = 3.35$, 4.35, 7.35, 11.35 cm). The MSSS model was omitted from Figure 10 since the five-points LSI model produced results identical with the MSSS approach. In Figure 10, the view factor and RAD-LSI yield very similar results in the region near the lamp. However, the agreement between these two models decreases with increasing radial distance. In this study, the view factor and RAD-LSI models utilize the same attenuation factor calculation (Equation 22b), which only accounts for the bending of light due to refraction and absorption effects. The only difference between these two models was in their calculation for fluence rate without refraction, reflection and absorption effects.

In the region close to the lamp, RAD-LSI will automatically select the RADIAL model that considered the lamp as a cylindrical object that emits light only in the radial direction. Similarly, the view factor approach also takes into account the cylindrical geometry of the lamp using a more complicated relationship. The inclusion of the cylindrical geometry would explain the similar performance near the lamp surface. However, far from the lamp surface, RAD-LSI will select the LSI model, which treats the lamp as a summation of point sources. As a result, the disagreement between RAD-LSI and the view factor model will be more significant in the regions far from the lamp surface.

While the attenuation factor method seems to be a reasonable approach for modelling the fluence rate with reflection, refraction and absorption, the user must exercise care in its use. The bending and focus effect of refraction as well as the cosine function have their own

Downloaded from https://iwaponline.com/aqua/article-pdf/53/6/391/402516/391.pdf
by guest

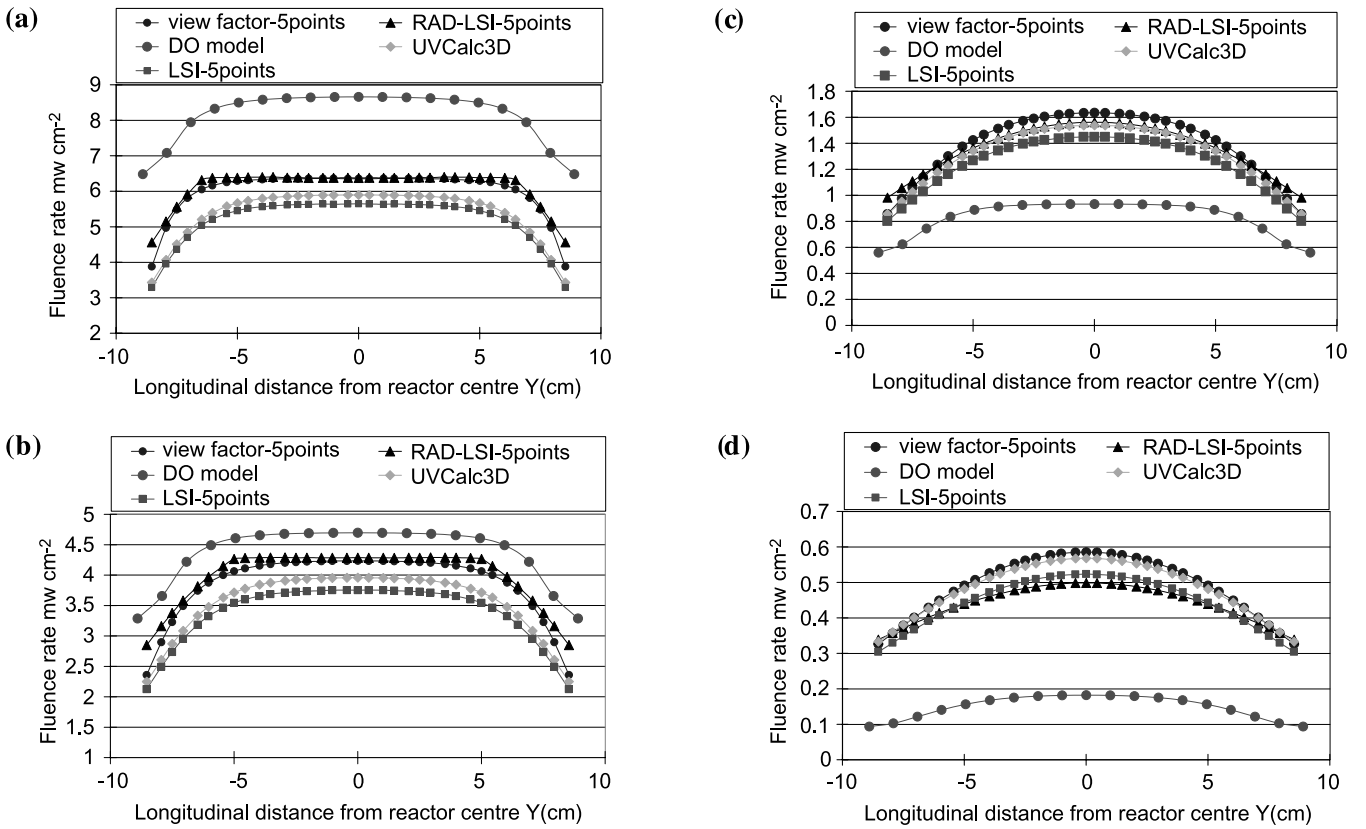

Figure 10 | Fluence rate longitudinal distribution, perpendicular distance from lamp: (a) x=3.35 cm, (b) x=4.35 cm, (c) x=7.35 cm, (d) x=11.35 cm.

individual influence on the shape of the fluence rate curve along the lamp length. A basic effect of refraction is light bending, which is caused by the position shift as UV light passes through air/quartz/water interfaces. The bending effect is also a prerequisite for the path length calculation, which is an integral part of the absorption effect in different media. As a result, the attenuation factor with the bending effect should be considered the minimum or basic refraction characterization level.

The focus effect is the second essential part of refraction, which will cause the central region of the longitudinal fluence rate distribution curve to be flatter and cause a sharp reduction in the fluence rate near the lamp ends. As illustrated in Figure 10a, the RAD-LSI and view factor models without the focus effect in the attenuation factor calculation already exhibit a flat profile in the central region of the lamp. This is due to their approximation of the lamp as a cylindrical surface that emits light primarily in the radial direction near the lamp surface. Consequently, the focus effect should not be included in the attenuation factor when using either the RAD-LSI or view factor models.

The cosine function was introduced to correct for the improper representation of a cylindrical lamp by the point source summation method. The results showed that a cost-efficient MSSS approach could be achieved using the LSI with an attenuation factor that includes not only the bending and focusing effects but also the cosine angle effect. The question that still remains is what model should be used in the evaluation of the UV reactor performance.

In the case of reviewing alternative design or process configurations, a reasonable approach would be to use the RAD-LSI or view factor model with an attenuation factor that includes absorption and light bending effects (Equation 22b). In the case of validating the model performance with biodosimetry tests or when the goal is to

Downloaded from https://iwaponline.com/aqua/article-pdf/53/6/391/402516/391.pdf
by guest

develop a numerical online fluence monitoring tool, an MSSS based fluence rate model should be applied to account for all the true physics of UV light. The MSSS fluence rate model could be used without significant cost in computational time and resources for reactors with a low number of lamps (i.e. six or less). With larger reactors utilizing more lamps, the LSI with the full attenuation factor (Equation 22c) or UVCalc3D could be used since it mimics the accuracy of the MSSS approach with a lower computational time. Moreover, the LSI with the full attenuation factor could further reduce the computational cost of the UVCalc3D model for reactors that contain multiple MP lamps. Overall, the fluence rate model that should be selected for simulations of UV reactor performance will depend on the ultimate use of the numerical data.

CONCLUSIONS

A detailed evaluation of several fluence rate distribution models has been performed. These models include the MPSS, MSSS, UVCalc3D, LSI, RAD-LSI, view factor and DO. The models were compared with experimental fluence rate measurements using spherical actinometers, which measure the fluence rate at specific points in space. Experimental fluence rate measurements were performed in air and in water at two different transmittances (77 and 88% at 254 nm). In addition, an MSSS approach was presented that includes the quartz sleeve thickness when calculating the refraction angle at air/quartz/water interfaces. Moreover, a cost effective approach was developed to simulate the MSSS by combining the LSI model with an attenuation factor that accounts for reflection, refraction, absorption and cosine angle effects. The results of this study show the following:

- RAD-LSI improved the performance of the original LSI model at the near lamp region in the air box study. Using a simple minimum function, the RAD-LSI utilizes the RADIAL fluence rate model in regions near the lamp surface and utilizes the LSI model in regions near the lamp ends and far from the lamp surface.
- The MSSS model, which includes the quartz sleeve thickness, and UVCalc3D, which applies a factor to account for the impact of the quartz sleeve on the fluence rate, produced similar results. This indicates that inclusion of the quartz sleeve thickness is insignificant, and that it can be approximated by a factor as calculated in UVCalc3D.
- The attenuation factor method combined with the LSI model was shown to be a reasonable compromise between computing time and accuracy with respect to the MSSS model. In addition, the attenuation factor can be incorporated into the view factor and RAD-LSI models to account for reflection, the bending effects of refraction and absorption effects.
- RAD-LSI and view factor predicted similar fluence rate distribution profiles near the lamp surface. However, the RAD-LSI model tends to predict a lower fluence rate than the view factor model with increasing radial distance.
- The DO model was found to significantly over-predict the fluence rate near the lamp surface and under-predict the fluence rate in regions far from the lamp surface because it did not incorporate the effects of refraction.
- The selection of bending and focus effect as well as the cosine angle in the attenuation factor calculation depends on the different models used. The bending effect is crucial for all models. However, the focus effect and cosine angle correction is only suggested with use in the LSI model.

ACKNOWLEDGEMENTS

This research was funded by a grant from AWWA Research Foundation no. 2682.

REFERENCES

Akehata, T. & Shirai, T. 1972 Effect of light-source characteristics on the performance of circular annular photochemical reactor. *J. Chem. Engng Japan* **5**(4), 385–391.

Downloaded from https://iwaponline.com/aqua/article-pdf/53/6/391/402516/391.pdf
by guest

Baas, M. M. 1996 Latest advances in UV disinfection hydrodynamic simulation and relation to practical experiences. *Proceedings AQUATECH* 1996, Amsterdam.

Blatchley, E. R. III 1997 Numerical modelling of UV intensity: application to collimated-beam reactors and continuous-flow systems. *Wat. Res.* **31**, 2205–2218.

Bolton, J. R. 2000 Calculation of ultraviolet fluence rate distribution in an annular reactor: significance of refraction and reflection. *Wat. Res.* **34**(13), 3315–3324.

Bolton, J. R. 2001 *Ultraviolet Application Handbook*. Bolton Photoscience Inc., Ontario, Canada.

Bolton, J. R., Dussert, B., Bukhari, Z., Hargy, T. & Clancy, J. L. 1998 Inactivation of *Cryptosporidium parvum* by medium-pressure ultraviolet light in finished drinking water. *Proceedings AWWA 1998 Annual Conference*, Dallas, Texas, vol. A, pp. 389–403.

Bukhari, Z., Hargy, T. M., Bolton, J. R., Dussert, B. & Clancy, J. L. 1999 Medium pressure UV light for oocyst inactivation. *J. Am. Wat. Wks Assoc.* **91**, 86–94.

Craik, S. A., Weldon, D., Finch, G. R., Bolton, J. R. & Belosevic, M. 2001 Inactivation of *Cryptosporidium parvum* oocysts using medium-and low-pressure ultraviolet radiation. *Wat. Res*. **35**(6), 1387–1398.

Ducoste, J. J., Liu, D. & Linden, K. 2003 Alternative approaches to modeling dose distribution and microbial inactivation in ultraviolet reactors: lagrangian vs eulerian. *J. Environ. Engng, ASCE* (submitted).

Fiveland, W. A. 1984 Discrete-ordinates solutions of the radiative transport equation for rectangular enclosures. *J. Heat Transfer* **106**, 699–705.

Hamilton, D. C. & Morgan, W. R. 1952 Radiant-interchange configuration factors. *NACA* Technical Note 2836.

Hsu, C. J. 1967 Shape factor equations for radiant heat transfer between two arbitrary sizes of rectangular planes. *Can. J. Chem. Engng* **45**, 58–60.

Jacob, S. M. & Dranoff, J. S. 1970 Light intensity profiles in a perfectly mixed photoreactor. *A.I.C.H.E. J.* **16**, 359–363.

Kowalski, W. J. & Bahnfleth, W. P. 2000 Effective UVGI system design through improved modelling. *ASHRAE Trans.* **106**(2), 4–15.

Kvalseth, T. O. 1985 Cautionary note about R^2. *Am. Statistician* **39**(4), 279–285.

Linden, K. G. & Mofidi, A. A. 1999 Measurement of UV irradiance: tools and considerations. *Proceedings, Water Quality Technology Conference*, AWWA, Tampa Bay, Florida, 1–3 November 1999.

Linden, K. G., Shin, G., Faubert, G., Cairns, W. & Sobsey, M. D. 2002 UV Disinfection of Giardia lamblia cysts in water. *Environ. Sci. Technol*. **36**(11), 2519–2522.

Liou, B. T. & Wu, C. Y. 1996 Radiative transfer in a multi-layer medium with fresnel interfaces. *Heat and Mass Transfer* **32**, 103–107.

Lu, X., Hsu, P. & Chai, J. C. 2003 Transient radiative transfer of light pulse propagation in three dimensional scattering media with finite volume method and integral equation method. *Proceedings ASME Summer Heat Transfer Conference* 2003, Las Vegas, Nevada.

Lyn, D. A., Chiu, K. & Blatchley, E. R. 1999 Numerical modeling of flow and disinfection in UV disinfection channels. *J. Environ. Engng, ASCE* **125**(1), 17.

Meyer-Arendt, J. R. 1984 *Introduction to Classical and Modern Optics*, 2nd edn. Prentice-Hall, Englewood cliffs, New Jersey, pp. 300–302.

Modest, M. F. 1993 *Radiative Heat Transfer.* McGraw-Hill, New York.

Rahn, R. O. 1997 Potassium iodide as a chemical actinometer for 254 nm radiation: use of iodate as an electron scavenger. *Photochem. Photobiol*. **66**(4), 450.

Rahn, R. O., Stefan, M. I. & Bolton, J. R. 2000 The iodide/iodate actinometer in UV disinfection: characteristics and use in the determination of the fluence rate distribution in UV Reactors. In *Proceedings Water Quality Technology Conference*, November 2000, Salt Lake City, Utah (CDROM published by the American Water Works Association, 6666 West Quincy Ave, Denver, CO 80235, USA).

Sommer, R., Cabaj, A., Sandu, T. & Lhotsky, M. (1999) Measurement of UV radiation using suspensions of microorganisms. *J. Photochem. Photobiol. B: Biol.* **53**, 1–6.

Stamnes, K., Chee Tsay, S., Wiscombe, W. & Jayaweera, K. 1988 Numerically stable algorithm for discrete-ordinate-method radiative transfer in multiple scattering and emitting layered media. *Appl. Opt*. **27**(12), 2502–2509.

Stefan, M. I., Rahn, R. O. & Bolton, J. R. 2001 Use of the iodide/iodate actinometer together with spherical cells for determination of the fluence rate distribution in UV reactors: validation of the mathematical model. *Proceedings 1st International Congress Ultraviolet Technology*. CDROM, International Ultraviolet Association, Washington, DC.

Tan, Z. M. & Hsu, P. F. 2001 An integral formulation of transient radiative transfer. *J. Heat Transfer* **123**(6), 466–475.

Tan, Z. M. & Hsu, P. F. 2002 Transient radiative transfer in three dimensional homogeneous and non-homogeneous participating media. *J. Quantve Spectrosc. Radiat. Transfer* **73**, 181–194.

First received 24 September 2003; accepted in revised form 20 March 2004

Downloaded from https://iwaponline.com/aqua/article-pdf/53/6/391/402516/391.pdf
by guest